Available online at www.sciencedirect.com
ScienceDirect
Journal of Nuclear Materials 363–365 (2007) 1179–1183
journal of nuclear materials
www.elsevier.com/locate/jnucmat

Be–W alloy formation in static and divertor-plasma simulator experiments

M.J. Baldwin [a,*], R.P. Doerner [a], D. Nishijima [a], D. Buchenauer [b], W.M. Clift [b], R.A. Causey [b], K. Schmid [c]

[a] University of California at San Diego, CA 92093, USA
[b] Sandia National Laboratories, Livermore, CA 94550, USA
[c] Max-Planck Institut für Plasmaphysik, Garching, Germany

Abstract

Collaborative Be–W interaction experiments conducted at UC-San Diego PISCES Laboratory, and Sandia National Laboratories, Livermore, CA (SNL/CA), are reported. In the divertor-plasma simulator PISCES–B, W targets are exposed to Be seeded D_2 plasma in the temperature range 1070–1320 K. All reveal the formation of surface Be–W alloying. The alloy reaction rate is found to increase with surface temperature in the range 1023–1123 K in SNL vacuum-deposition phase formation experiments. In both sets of experiments the efficiency of surface alloying is found to depend on the availability of surface deposited Be. This availability is reduced by evaporation at high temperature, and also by plasma re-erosion in the case of PISCES–B targets. Surface analysis of targets using Auger electron spectroscopy (AES), wavelength dispersive X-ray spectroscopy (WDS), and X-ray diffraction (XRD) reveals $Be_{12}W$ as the dominant alloy composition where Be surface availability is optimal.

PACS: 52.40.Hf

Keywords: Beryllium; ITER; Mixed materials; PISCES–B; Tungsten

1. Introduction

The current ITER design makes use of Be, W and C (graphite) plasma facing component (PFC) materials [1]. In the near future, JET will undertake 'ITER-like wall' experiments where a combination of these materials is also to be attempted [2]. In both reactors, a Be first wall and a full or partial, W divertor will be common and the divertor-plasma is expected to contain ionized Be due to first-wall erosion. In ITER, the fraction of Be in the plasma, $f_{Be^+} \approx n_{Be^+}/n_e$, is expected to be in the range 0.01–0.10 [3], leading to an incident flux as high as $\sim$100–1000 ML s^{-1} of Be on ITER divertor surfaces.

A real concern, where Be and W interact, is the formation of Be–W alloy. All Be–W alloy compositions have partial equilibrium liquid phases at, or

* Corresponding author. Tel.: +1 858 534 1655.
E-mail address: mbaldwin@ferp.ucsd.edu (M.J. Baldwin).

0022-3115/$ - see front matter © 2007 Elsevier B.V. All rights reserved.
doi:10.1016/j.jnucmat.2007.01.151

significantly below, the melting point of W (3695 K) [4]. For dissolved Be levels ~5–67 at.%, a liquid phase component precipitates above ~2370 K. With increasing Be content, the stable alloy stiochiometries Be_2W, $Be_{12}W$ and $Be_{22}W$ are known to form, and these have molten phase components at ~2520 K, ~1780 K, and ~1600 K respectively.While the operational temperature range for ITER W PFCs is expected to be lower than this, at 900–1300 K [5], localized hot regions and the effects of ELMs may see surface temperature excursions well into the Be–W partial liquid phase regime. Then, should Be transport into the W bulk be rapid enough that alloy formation is not limited to the near surface, a potentially serious problem that could affect reactor operation and PFC lifetime is presented.

2. Experiments

2.1. UC–PISCES

Plasma–materials interactions (PMI) studies are conducted in the PISCES–B divertor-plasma simulator. PISCES–B produces intense plasmas through D_2 ($n_e \sim 10^{18}$–$10^{19}\,m^{-3}$, $T_e \sim 6$–12 eV as measured by Langmuir probe) that can be seeded with controlled amounts of Be using a neutral Be atom source [3,6]. Polished ITER grade W targets, 25 mm in diameter and 1 mm thick are exposed to high-flux ($\Gamma_{D^+} = 0.2$–1.0×10^{23} ions $m^{-2}\,s^{-1}$) plasma over ~3600 s with f_{Be^+} set in the range 0.0005–0.008. Plasma conditions and target temperature, T_s, are kept fixed and a temperature range spanning 1070–1320 K was explored. Target bias regimes of floating and −75 V were used to explore the role of energetic ion bombardment. The energy of impacting ions is estimated from the target bias, $\langle E_{ions}\rangle \approx V_{bias} - 2kT_e$. Subsequent to exposure, targets are analyzed using scanning electron microscopy (SEM) and a wavelength dispersive X-ray spectrometer (WDS).

2.2. SNL vacuum deposition experiments

Phase formation and reaction kinetics experiments are conducted in vacuum ($<2 \times 10^{-6}$ Torr) by depositing Be on to W targets (similar to those in Section 2.1) with a high-temperature (up to 1750 K) effusion cell. A thermocouple and optical pyrometer are used to determine the surface temperature during both a 1 h pre-anneal at 1223 K and in preparation for the deposition (only the thermocouple is used during the deposition). The average deposition rate for Be is measured on a cooled Si target. Full target surface coverage in Be (i.e., net Be deposition) was achieved with fluxes of $2 \times 10^{19}\,m^{-2}\,s^{-1}$ at 1023 K and $5 \times 10^{19}\,m^{-2}\,s^{-1}$ at 1123 K. An exposure conducted at 1223 K did not show complete Be coverage up to fluxes of $10^{20}\,m^{-2}\,s^{-1}$.

3. Results and discussion

3.1. PMI Be–W alloy formation (PISCES–B)

Fig. 1 shows a selection of W targets that were exposed to various Be seeded plasmas in PISCES–B. All of these targets show evidence of the formation of a Be–W alloy surface. By way of comparison, the images in Fig. 1 point to the availability of surface Be as a key factor in Be–W alloy production.

In the exposed-target cross-section of Fig. 1(a), a $Be_{12}W$ layer ~0.3 μm thick, has formed at the interface between the W surface and a ~5 μm thick layer of Be surface deposits. This exposure was conducted at 1070 K with a floating target bias, so that the temperature and ion energy were low enough that the deposited Be did not evaporate, or erode by sputtering.

In comparison, Fig. 1(b) shows the surface of a target exposed under similar conditions except that the ion energy is ~60 eV. Despite the increased f_{Be^+} in this case, there is no apparent layer of deposited Be, as in Fig. 1(a). The absence of Be deposits can be explained by sputtering. Further, the loss of available surface Be results in only small ~0.3 μm high nucleation zones of Be–W alloy that are close to the composition $Be_{12}W$ distributed over a W rich surface as measured by WDS analysis. Cross-sectional analysis did not reveal significant Be below the surface.

Comparing the target cross-section in Fig. 1(c) to 1(a) reveals the effect of evaporation, which also acts to inhibit the formation of Be deposits. This target had a higher exposure temperature of 1150 K and was also floating. The surface of the target has developed a $Be_{12}W$ alloy layer ~1 μm in thickness. This layer accommodates $\sim 1 \times 10^{22}\,m^{-2}$ Be atoms. The fluence of incident Be ions during plasma exposure was larger, $9.7 \times 10^{22}\,m^{-2}$. The difference is in reasonable agreement with the number of Be atoms

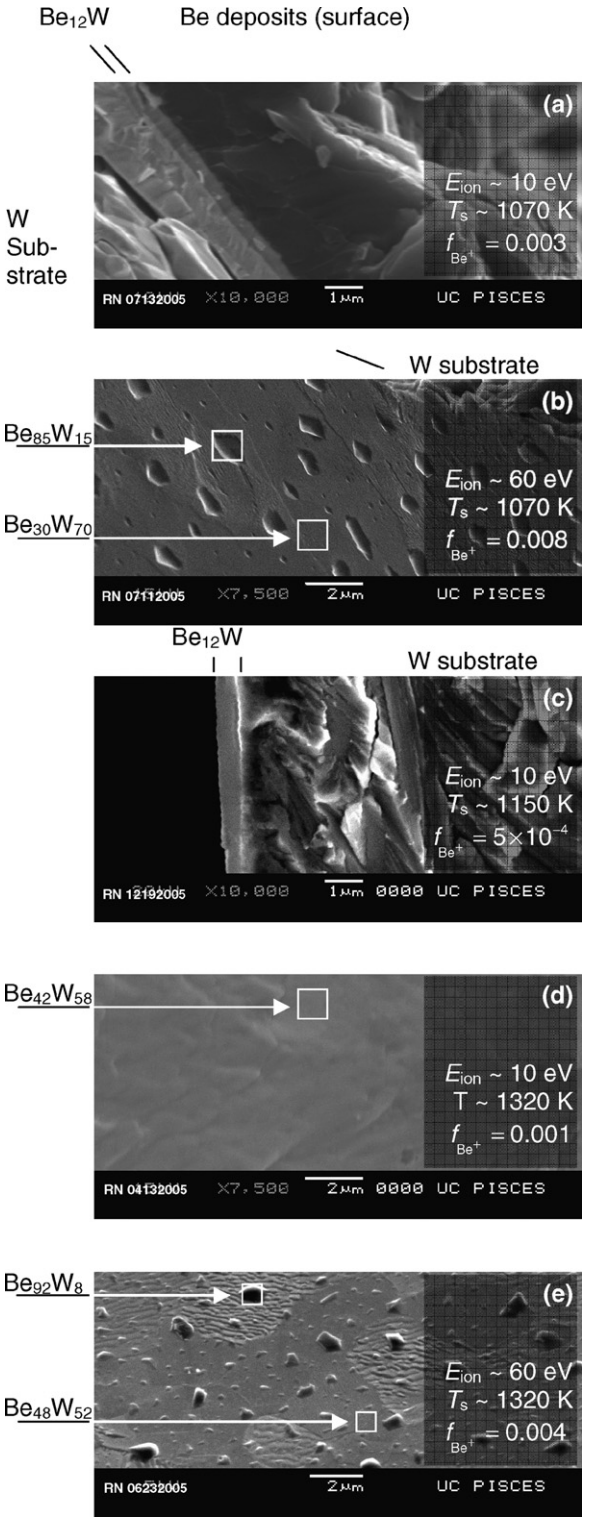

Fig. 1. (a–e) SEM images of W targets exposed to Be seeded D_2 plasma in PISCES–B. Compositional data provided by standardized WDS analysis at 5 kV. (a) and (c) are cross-sections, (b), (d) and (e) are the plasma exposed surfaces.

that evaporate from a Be surface at 1150 K over 3600 s [7] (6.9×10^{22} m^{-2}).

Comparing Fig. 1(d) to 1(c), the even higher exposure temperature of 1320 K seems to be detrimental to alloy formation. The surface composition is below the stoichiometry for even Be_2W, and in spite of an expected increase in mobility for Be in the bulk, cross-sectional analysis revealed little evidence for any Be below the surface. On this target it seems likely that evaporation hindered the Be–W interaction; the evaporative flux of Be at 1320 K is 1.5×10^{21} m^{-2} s^{-1} [7], much greater than the inbound flux of $\sim 3.5 \times 10^{19}$ m^{-2} s^{-1} during plasma exposure. However, under the same conditions as in Fig. 1(d) but with ion bombardment at 60 eV, alloy nucleation zones are observed. Fig. 1(e) shows this, $Be_{12}W$ surface nucleation over an almost identical surface to that of Fig. 1(d). The implantation of Be just beneath the surface, or additional energy of the incoming Be ions, is suspected as the contributing factor in this case.

A key message of Fig. 1 is that the availability of surface Be is paramount for Be–W alloy formation and that Be erosion by ions, and/or evaporation at high temperature, reduces availability. A surface particle balance model is useful for predicting the PMI conditions under which a deposited Be layer forms. Plasma deposited Be on the hot W surface can be eroded, redeposited, evaporated or enter the bulk. Net Be layer growth is observed whenever the incident Be flux, $J^{\mathrm{Be}}_{\mathrm{in}}$, exceeds that lost, $J^{\mathrm{Be}}_{\mathrm{out}}$. These quantities are given by

$$J^{\mathrm{Be}}_{\mathrm{in}} = f_{\mathrm{Be}^+}\Gamma_{\mathrm{D}^+}(1-R_{\mathrm{r}}), \tag{1a}$$

$$J^{\mathrm{Be}}_{\mathrm{out}} = Y_{\mathrm{D}\to\mathrm{Be}}\Gamma_{\mathrm{D}^+}(1-R_{\mathrm{d}}) + f_{\mathrm{Be}^+}Y_{\mathrm{Be}\to\mathrm{Be}}\Gamma_{\mathrm{D}^+}(1-R_{\mathrm{d}}) + \Gamma_{\mathrm{e}}(1-R_{\mathrm{e}}) + \xi(T_{\mathrm{s}}), \tag{1b}$$

where R_{r} is the reflection coefficient for Be on W, $Y_{\mathrm{D}\to\mathrm{Be}}$ and $Y_{\mathrm{Be}\to\mathrm{Be}}$ are the sputter yields for D^+ and Be ions on Be, R_{d} and R_{e} are redeposition fractions for sputtered and evaporated Be, Γ_{e} is the evaporative flux of Be from the surface, and $\xi(T_{\mathrm{s}})$ is a loss flux into the bulk due to either diffusion [8] or chemical reaction [9]. The value of f_{Be^+} when Eqs. (1a) and (1b) are equated is the minimum 'critical' Be fraction in the plasma that will lead to the formation of a full Be deposited layer. At this critical value, alloy formation might be expected to be most efficient (It is important to note however, that the prediction of this simple model relies critically on the yield values, and that these values, for a deposited Be layer on W, may be different than that

for pure crystalline Be.). With reference to the targets and PMI conditions in Fig. 1(a)–(e), these critical values, $f_{Be^+(critical)}$ are 0.2×10^{-4}, 0.0480, 1.0×10^{-4}, 0.0050 and 0.0530, respectively, calculated using sputter yield and reflection coefficients in [10], redeposition fractions in [3], and ignoring the reaction term, $\xi(T_s)$. In spite of the simplicity of the model and assumptions, somewhat good agreement is observed with the observations in Fig. 1. Only those targets where f_{Be^+} was greater than $f_{Be^+(critical)}$ (i.e. Fig. 1(a) and (c)) had full alloy layer growth.

3.2. Be–W reactions in vacuum (SNL)

To investigate the growth of Be–W alloy layers over time, an atomic flux of Be was deposited onto W substrates at temperatures of 1023 K and 1123 K for 1 and 4 h. The structure of the resulting layers was similar to those in Fig. 1(a), having net Be on the surface (full Be coverage) with a reacted layer between the Be and the W. Auger Line scans of a 3600 s exposed deposition target at 1123 K showed a uniform reacted layer ~1 μm thick of composition, $Be_{12}W$. A small amount of Be (3.5 at.%) was observed in the W below the layer, consistent with the solubility limit.

Fig. 2 shows the dependence of the reaction layer thickness on time and temperature, along with fits based on a diffusional behavior to the growth front (i.e., $d^2 = 4Dt$, where d is the reacted layer thickness, D is the diffusion coefficient, and t is the reaction time). Also shown is a target grown for 3600 s at 1223 K, but for which only partial Be coverage was achieved. The line scan for this target indicated an alloy layer composition closer to $Be_{50}W_{50}$.

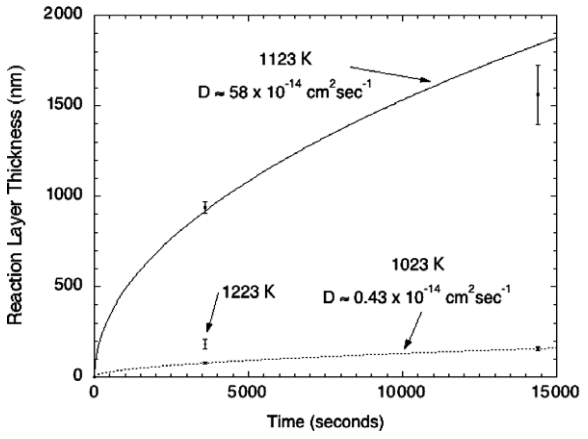

Fig. 2. Reaction layer thickness as a function of time (points with error bars), with fits based on diffusional reaction front behavior (solid and dashed curves). The data point at 1223 K was not obtained under Be rich conditions.

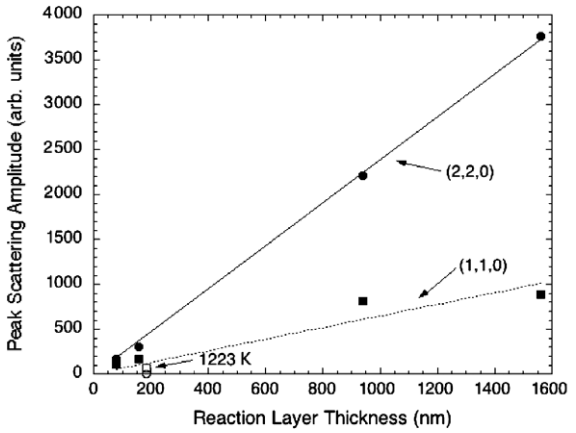

Fig. 3. Scaling of (1,1,0) and (2,2,0) diffraction peaks with reaction layer thickness. The data point at 1223 K was not obtained with full Be surface coverage.

XRD was used to investigate the structure of the reacted alloy layers. Fig. 3 shows the intensity of two low-angle $Be_{12}W$ peaks ($2\theta = 17.306°$ & 35.023°) as a function of reacted layer thickness. The scaling of the higher intensity peak (2,2,0) correlates well with the reacted layer thickness indicative of uniform structural arrangement into the alloy phase throughout the reacted layer. For the target at 1223 K, which had low Be availability on the surface, the XRD peaks are almost absent.

4. Conclusion

W targets exposed at 1070–1320 K to PISCES–B Be seeded D_2 plasma reveal the formation of ~Be_2W and $Be_{12}W$ surface alloys. At SNL, vacuum deposition experiments indicate increased $Be_{12}W$ reaction with temperature in the range 1023–1123 K. The reacted layer thickness in PISCES–B PMI and SNL experiments agree well over this temperature range when adequate surface Be availability is maintained. In PMI experiments, the loss of Be from the surface due to re-erosion and/or evaporation at high temperature, is found to inhibit the formation of the alloy phase. AES, XRD and WDS surface analysis methods indicate that $Be_{12}W$ dominates when Be availability is adequate.

In ITER, a significant part of W divertor area is expected to operate at around 900 K. At this temperature, the growth of reacted alloy should not

be severe as suggested by Figs. 2 and 3 and data in the literature [9,11,12]. At higher temperature both the USCD and SNL Be–W experiments show that alloying proceeds most efficiently when the availability of surface Be is optimal. This availability, in terms of net layer growth of Be deposits, is reasonably predicted with the zero dimensional PMI surface model of Section 3.1. At the ITER upper limit temperature of 1300 K these experiments show that it is difficult to achieve net Be layer growth due to evaporative loss. However, in ITER, where the plasma beryllium fraction and redeposition rates will be much greater, net Be layer growth will be sustained at considerably higher temperature than is achieved in the current experiments. This, coupled with transient high temperature thermal loads due to ELMing may lead to more rapid Be–W alloying effects. These phenomena are soon to be explored in PISCES–B using a new feature that allows target pulsing with transient heat loads [13] during plasma operation.

Acknowledgements

The authors gratefully acknowledge PISCES–B and SNL technical staff. This work is supported by USDoE Contracts: DOE DE-FG03-95ER-54301 & DE-AC04-94AL85000.

References

[1] G. Federici, P. Andrew, P. Barabaschi, et al., J. Nucl. Mater. 313–316 (2003) 11.
[2] C. Grisolia, S. Rosanvallon, P. Coad, et al., Fusion Eng. Des. 81 (2006) 149.
[3] R. Doerner, M.J. Baldwin, K. Schmid, Physica Scripta T111 (2004) 75.
[4] H. Okamoto, L.E. Tanner, in: S.V. Nagendra Naidu, P. Ramo Rao (Eds.), Phase Diagrams of Binary Tungsten Alloys, Indian Institute of Metals, Calcutta, 1991.
[5] G. Federici, R.A. Anderl, R. Andrew, et al., J. Nucl. Mater. 266–269 (1999) 14.
[6] M.J. Baldwin, R.P. Doerner, Nucl. Fusion 46 (4) (2006) 444.
[7] D.R. Lide, CRC Handbook of Chemistry and Physics, Internet Version (2005).
[8] Linsmeir et al., J. Nucl. Mater. these Proceedings.
[9] E. Vasina, A.S. Panov, Russ. Metall. (Metally) 1 (1974) 119.
[10] W. Eckstein, Calculated Sputtering, Reflection and Range Values, Max–Planck Institut für Plasmaphysik Report 9/17 (1998).
[11] R.P. Doerner, M.J. Baldwin, R.A. Causey, J Nucl. Mater. 342 (2005) 63.
[12] C.R. Watts, Int. J. Powder Metall. 4 (3) (1968) 49.
[13] J. Hanna, R. Doerner, R. Hernandez, R. Seraydarian, R. Pugno, Rev. Sci. Instrum. 77 (2006) 123503.